Positive- and negative-feedback regulations coordinate the dynamic behavior of the Ras-Raf-MEK-ERK signal transduction pathway

Sung-Young Shin[1,*], Oliver Rath[2,*], Sang-Mok Choo[3], Frances Fee[2], Brian McFerran[2,‡], Walter Kolch[2,4,§] and Kwang-Hyun Cho[1,§]

[1]Department of Bio and Brain Engineering and KI for the BioCentury, Korea Advanced Institute of Science and Technology (KAIST), Daejeon, Korea
[2]Beatson Institute for Cancer Research, Cancer Research UK, Glasgow, UK
[3]School of Electrical Engineering, University of Ulsan, Ulsan, Korea
[4]Institute of Biomedical and Life Science, University of Glasgow, Glasgow, UK

*These authors contributed equally to this work
‡Present address: Organon Labs, Newhouse, Motherwell, UK
§Authors for correspondence (e-mails: ckh@kaist.ac.kr; w.kolch@beatson.gla.ac.uk)

Accepted 12 October 2008
Journal of Cell Science 122, 425-435 Published by The Company of Biologists 2009
doi:10.1242/jcs.036319

Summary

The Ras-Raf-MEK-ERK pathway (or ERK pathway) is an important signal transduction system involved in the control of cell proliferation, survival and differentiation. However, the dynamic regulation of the pathway by positive- and negative-feedback mechanisms, in particular the functional role of Raf kinase inhibitor protein (RKIP) are still incompletely understood. RKIP is a physiological endogenous inhibitor of MEK phosphorylation by Raf kinases, but also participates in a positive-feedback loop in which ERK can inactivate RKIP. The aim of this study was to elucidate the hidden dynamics of these feedback mechanisms and to identify the functional role of RKIP through combined efforts of biochemical experiments and in silico simulations based on an experimentally validated mathematical model. We show that the negative-feedback loop from ERK to SOS plays a crucial role in generating an oscillatory behavior of ERK activity. The positive-feedback loop in which ERK functionally inactivates RKIP also enhances the oscillatory activation pattern of ERK. However, RKIP itself has an important role in inducing a switch-like behavior of MEK activity. When overexpressed, RKIP also causes delayed and reduced responses of ERK. Thus, positive- and negative-feedback loops and RKIP work together to shape the response pattern and dynamical characteristics of the ERK pathway.

Key words: Systems biology, ERK signaling pathway, RKIP, Feedback regulation, Dynamics, Mathematical modeling

Introduction

Signal transduction through the Ras-Raf-MEK-ERK pathway (or ERK pathway for short) is essential for many cellular processes, including growth, cell-cycle progression, differentiation, and apoptosis (Kolch, 2000; Kolch, 2002; Kolch, 2005; Wellbrock et al., 2004). The activation of this pathway is well characterized (for recent reviews, see Kolch, 2005; Wellbrock et al., 2004). Typically, it is initiated by the growth-factor-induced recruitment of the SOS-Grb2 complex to the plasma membrane. The SOS-Grb2 complex catalyzes the transformation of an inactive GDP-bound form of Ras (Ras-GDP) into its active GTP-bound form (Ras-GTP). Ras-GTP binds the Raf-1 kinase with high affinity, which induces the recruitment of Raf-1 from the cytosol to the cell membrane. Activated Raf-1 phosphorylates and activates mitogen-activated protein kinase kinase (MEK), a kinase that in turn phosphorylates and activates mitogen-activated protein kinase (MAPK). Activated extracellular signal-regulated kinases (ERKs) regulate more than 70 substrates including nuclear transcription factors. Thus ERKs have a profound influence on many biochemical processes in different subcellular compartments, and in combination with other pathways regulate cellular physiology (Kolch et al., 2005). The ERK pathway and its regulation by RKIP are schematically shown in Fig. 1.

Activated ERK feeds back to the pathway activation at several levels (Kolch et al., 2005). ERK exerts a negative feedback by interfering with Ras activation through SOS phosphorylation (Dong et al., 1996). Waters and colleagues showed that despite the continuous stimulation of receptor tyrosine kinase activity, Ras activity is transient and it returns to inactive Ras-GDP within 5 minutes (Waters et al., 1995a). They further showed that insulin stimulation resulted in a decreased affinity of SOS to Grb2, whereas the dissociation of SOS from Grb2 did not affect the interactions between Grb2 and tyrosine-phosphorylated Shc (Waters et al., 1995b). The dissociation of the Grb2-SOS complex is due to phosphorylation of SOS by activated ERK (Langlois et al., 1995) or the ERK downstream kinase RSK2 (Douville and Downward, 1997).

In addition, the physical interaction of MEK with Raf-1 required for phosphorylation of MEK at the activating sites S218 and S222 is highly regulated. In response to cell adhesion, the serine/threonine-protein kinase PAK1, acting downstream of the small G-protein Rac, phosphorylates the MEK proline-rich sequence (PRS) at S298, and PAK3 was reported to phosphorylate Raf-1 at S338 (Eblen et al., 2004). The phosphorylation of MEK at S298 by PAK1 enhances its interaction with Raf-1, whereas ERK-feedback phosphorylation of MEK1 on T292 inhibits the

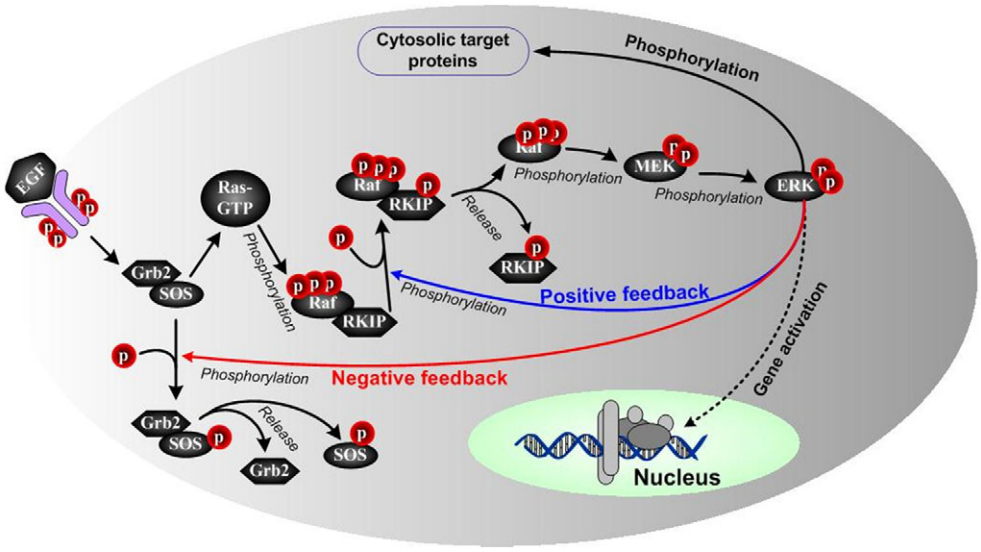

Fig. 1. The Ras-Raf-MEK-ERK signaling pathway and its feedback regulation mechanism. Activated ERK (ppERK) triggers two major feedback loops: the positive-feedback loop resulting from inactivation of the inhibitory protein RKIP and the negative-feedback loop formed by inactivation of the Ras activating exchange factor complex Grb2-SOS.

ability of PAK1 to phosphorylate S298 of MEK and thereby interferes with MEK-ERK complex formation stimulated by Rac (Eblen et al., 2004). The interaction between Raf and MEK is also regulated by Raf kinase inhibitor protein (RKIP), a protein that binds to both Raf and MEK preventing their physical interaction (Yeung et al., 2000; Yeung et al., 1999). As a consequence, the overexpression of RKIP suppresses the activation of MEK and ERK and the induction of AP-1-dependent transcription (Yeung et al., 1999). By contrast, the downregulation of endogenous RKIP induces the activation of MEK and ERK, and enhances AP-1-dependent transcription. RKIP does not affect Raf-1 catalytic activity in general, but specifically interferes with the phosphorylation of its substrate MEK (Yeung et al., 2000). According to enzyme kinetic analysis, RKIP acts like a competitive inhibitor of MEK phosphorylation (Yeung et al., 2000). Yeung and co-workers demonstrated that stimulation of COS-1 cells with 12-O-tetradecanoylphorbol-13-acetate (TPA) plus epidermal growth factor receptor (EGF) caused an increase of ERK pathway activity, which was correlated with the decrease of RKIP association with Raf-1 (Yeung et al., 2000). At later time points, as ERK pathway activity declined, RKIP binding to Raf-1 increased again. The association of Raf-1 with RKIP is regulated by several mechanisms that involve RKIP phosphorylation. RKIP dissociation from Raf-1 is triggered by phosphorylation of RKIP on S153 through protein kinase C (PKC) (Corbit et al., 2003) or putatively through ERK (Cho et al., 2003a). In the latter case, a positive-feedback loop is formed and thereby ERK-mediated RKIP phosphorylation counteracts the inhibitory function of RKIP. However, direct evidence of ERK-mediated RKIP phosphorylation has not previously been reported.

RKIP is a member of the phosphatidylethanolamine-binding protein (PEBP) family and has wide tissue expression in a variety of different mammalian species such as monkey, rat, chicken and human (Keller et al., 2004). Its effect on the ERK pathway was the first to be discovered (Yeung et al., 1999); however, RKIP proved to be a multifunctional protein. RKIP also antagonizes the activation of the transcription factor nuclear factor kappa B (NF-κB) in response to tumor necrosis factor alpha (TNFα) and interleukin-1 beta (IL-1β) stimulation (Hagan et al., 2005b; Keller et al., 2004). In addition, RKIP is a physiological inhibitor of G-protein-coupled receptor kinase (GRK2). After stimulation of the G-protein-coupled receptor (GPCR), RKIP dissociates from Raf-1 and associates with GRK2 and subsequently blocks its activity. This switch is triggered by PKC-dependent phosphorylation of RKIP on S153, and serves to directly connect the ERK pathway with GPCR signaling.

RKIP has been reported to play various pathophysiological roles in non-neoplastic and neoplastic diseases (Keller et al., 2004). For instance, RKIP and its cleavage product, hippocampal cholinergic neurostimulating peptide (HCNP) were reported to be associated with Alzheimer's disease and dementia (Keller et al., 2004). However, the best documented role of RKIP is in cancer. Here, RKIP has been identified to have the properties of a metastasis suppressor gene. Fu and colleagues demonstrated that the decrease of RKIP expression in primary malignant prostate tumors is associated with the increased capability of prostate cancer cells to invade and form distant metastases (Fu et al., 2003). Similar results were reported in melanoma (Schuierer et al., 2004), breast cancers (Hagan et al., 2005a) and colorectal cancers (Al-Mulla et al., 2006). In addition, RKIP might also mediate the sensitivity of cancer cells to chemotherapeutic drugs, because RKIP sensitizes prostate and breast cancer cells to drug-induced apoptosis (Chatterjee et al., 2004). However, despite these very important roles of RKIP, the regulation mechanisms of RKIP are not yet fully understood.

In all the cancer studies cited above, the role of RKIP could be closely linked to its protein expression levels. However, despite their obvious importance, it is currently unclear how different levels of RKIP protein expression impact its function. The existence of multiple feedback mechanisms in the ERK pathway is likely to profoundly affect this relationship in a non-linear fashion. Therefore, we investigated the role of RKIP with particular emphasis on its function in the feedback regulation. In this study, we consider two major feedback loops that are both triggered by activated ERK: (1) the positive-feedback loop that results from the inactivation of the inhibitor RKIP; and (2) the negative-feedback loop that is generated by the inactivation of the Ras-activating exchange factor complex Grb2-SOS. Although there are several theoretical studies on the feedback dynamics of the ERK pathway (Kholodenko, 2000; Markevich et al., 2004), the dynamics of multiple feedback

mechanisms, including RKIP, have not yet been investigated. The aim of this study was to elucidate the hidden dynamics of the positive and negative feedback mechanisms and to identify the functional role of RKIP in the ERK pathway through combined efforts of biochemical in vitro experiments and in silico simulations. A mathematical model was constructed based on experimental biochemical data obtained in vitro and from mammalian COS-1 cells.

Our results show that the negative-feedback loop of the ERK pathway has a crucial role in generating an oscillatory behavior of ERK activity. This behavior has been predicted by profound theoretical considerations, but has only recently been shown experimentally (Nakayama et al., 2008), albeit without an analysis of its origin. The positive-feedback loop in which ERK functionally inactivates RKIP enhances the oscillatory pattern of ERK dynamics. The positive-feedback loop also has an important role in inducing a switch-like behavior of the phosphorylated MEK in response to gradually increasing RKIP. RKIP, through its function as inhibitor, also causes delayed and decreased responses of ERK. Thus, RKIP, in conjunction with the positive- and negative-feedback loops, critically determines the dynamic characteristics of ERK activity.

Results

ERK-mediated RKIP phosphorylation generates a positive-feedback loop

In a previous study, we showed that the activity of the ERK pathway increases as the RKIP association with Raf-1 decreases in response to TPA plus EGF stimulation in COS-1 cells (Yeung et al., 1999). However, the underlying mechanism is still not fully understood. We have previously, mainly on theoretical grounds, postulated that the ERK-mediated RKIP phosphorylation counteracts the inhibitory function of RKIP (Cho et al., 2003a). Therefore, we conducted experiments to test this hypothesis directly. First, we tested whether RKIP is a substrate for ERK. For this purpose purified recombinant RKIP was incubated with purified Raf-1, MEK and ERK proteins under kinase assay conditions, either individually or in combination. Raf-1 was expressed in Sf-9 insect cells on its own or coexpressed with activated H-RasV12 and Lck to activate it, as previously described (Hafner et al., 1994). MEK and ERK were produced in *E. coli* as described (Gardner et al., 1994), and activated by preincubation with activated Raf-1 as indicated. Although neither Raf-1 nor MEK could phosphorylate RKIP, ERK phosphorylated RKIP and phosphorylation increased when ERK had been activated by preincubation with Raf-1 and MEK (Fig. 2A). Two-dimensional phosphopeptide mapping revealed the phosphorylation of one major and several minor sites (data not shown). Based on the predicted migration of phosphopeptides (http://xylian.igh.cnrs.fr/mobility7.php), selected candidate residues were mutated and the resulting mutants were tested as ERK substrates. The mutation of S99 severely reduced phosphorylation by ERK (Fig. 2B). Thus, the ERK phosphorylation site is distinct from S153, which is phosphorylated by PKC (Corbit et al., 2003), and although the PKC site represents a site for crosstalk, the ERK site generates the possibility of a feedback loop.

Therefore, we examined the functional effects of this feedback in in vitro kinase assays. To this end we assayed how MEK phosphorylation by Raf-1 was affected by increasing amounts of RKIP in the presence or absence of ERK (Fig. 2C). Activated Raf-1 was produced in Sf-9 cells (Hafner et al., 1994) and incubated with MEK under kinase assay conditions. The addition of increasing amounts of RKIP resulted in a stoichiometric inhibition of MEK phosphorylation, as expected from the known mode of action of RKIP as stoichiometric inhibitor of Raf-1-mediated MEK phosphorylation. By contrast, when recombinant ERK was also added to the reaction, inhibition of MEK phosphorylation became more sustained before steeply dropping at high RKIP concentrations. This behavior is consistent with a positive-feedback loop, where ERK inhibits the RKIP inhibitor. To inhibit MEK phosphorylation, RKIP must bind to Raf-1 (Yeung et al., 2000). Therefore, we tested whether ERK phosphorylation influences RKIP binding to Raf-1. For this purpose GST-tagged Raf-1, or GST as a control, were expressed in Sf-9 insect cells and purified by adsorption to glutathione-Sepharose beads. The GST or GST-Raf-1 beads were subsequently incubated with recombinant RKIP that had been phosphorylated by ERK in the presence of [γ-^{32}P]ATP. Bound RKIP was detected by western blotting and phosphorylation by autoradiography (Fig. 2D). Under in vitro conditions, phosphorylation of RKIP by ERK is not complete and the preparation also contains unphosphorylated ERK. No phosphorylated RKIP was detected binding to GST-Raf-1 beads – only the unphosphorylated fraction could bind. This confirms that ERK phosphorylation of RKIP interferes with Raf-1 binding and provides a mechanism for the effects of RKIP phosphorylation by ERK. Taken together with the previous experimental results (Yeung et al., 1999), these data prove that ERK-mediated RKIP phosphorylation forms a positive-feedback loop in the ERK pathway.

Oscillatory behavior of ERK activity

Oscillations in ERK activity have been predicted based on theoretical considerations and recently shown experimentally (Nakayama et al., 2008), albeit without any suggestion of a mechanism. Such oscillations are usually not observed in short-term stimulation experiments. Therefore, we stimulated COS-1 cells with TPA, sampling 12 data points over an extended period of time (300 minutes). Under these conditions, slow oscillations of phospho-ERK (ppERK) levels were observed (Fig. 3A). However, owing to practical limitations of wet experimentation, it is difficult and tedious to sample at the high density of time points required to accurately determine the oscillation pattern. Therefore, we developed a new parameter-estimation method, a pseudo-random search algorithm (PRSA), which is described in the Materials and Methods. Briefly, the PSRA iteratively explores a constrained parameter space around an estimated value, but avoids getting trapped in local minima. Applying the PRSA to the sparse experimental ppERK values observed in Fig. 3A, we showed that the experimental data can be correlated with a dampened oscillation curve (Fig. 3B). To verify the robustness of our mathematical model to parameter variation, we carried out repeated simulations (n=50) over 30% random variation of parameters and confirmed that the oscillatory behavior of ERK activation is well preserved to such parameter variations.

Dynamic analysis of the positive- and negative-feedback mechanisms

Thus, the ERK pathway features both positive- and negative-feedback loops, which have essential roles in the regulation of system dynamics. To investigate the hidden dynamics of two feedback loops, we removed each feedback loop individually and simulated the model for persistent stimulations (300 minutes) and transient stimulations (30 minutes). In both cases, we maintained the same peak level of stimulation. When the pathway was

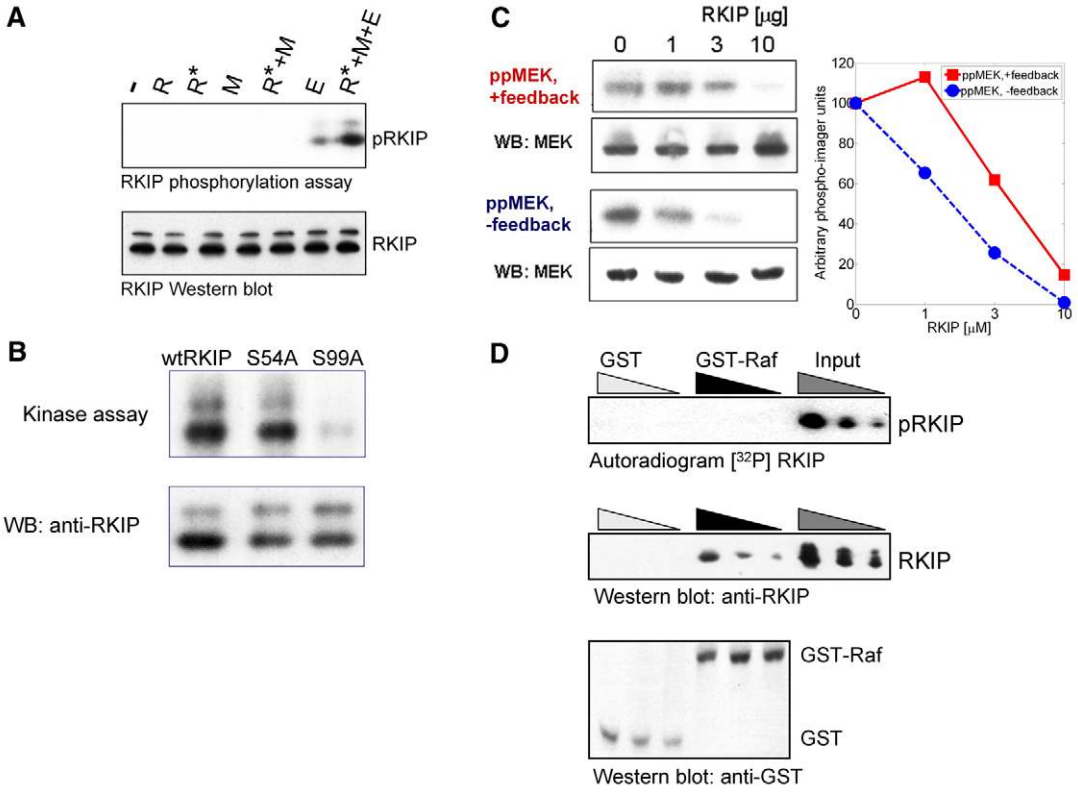

Fig. 2. ERK phosphorylates RKIP generating a positive-feedback loop. (A) RKIP is a substrate for ERK. Recombinantly produced purified RKIP protein was phosphorylated in vitro with purified Raf-1, MEK and ERK proteins exactly as described previously (Yeung et al., 2000). R, R*, M and E represent Raf-1, activated Raf-1, MEK and ERK, respectively. RKIP is phosphorylated only when ERK is present in the reaction. When ERK is activated by preincubation with activated Raf-1 and MEK (R*+M+E) RKIP phosphorylation is enhanced. (B) S99 of RKIP is an ERK phosphorylation site. Wild-type RKIP and the indicated mutants were expressed in *E. coli*, purified and phosphorylated by activated ERK in vitro. Mutation of S99 substantially reduces the phosphorylation of RKIP by ERK. (C) RKIP inhibitory function is inhibited by ERK phosphorylation generating a positive-feedback loop. Recombinant purified proteins were used to reconstitute the Raf-1–MEK–ERK phosphorylation cascade in vitro as described in the Materials and Methods section. MEK phosphorylation in the presence of increasing amounts of recombinant RKIP was assayed by ppMEK antibodies. '-feedback' indicates that MEK phosphorylation by Raf-1 was assayed in a reaction containing Raf-1, MEK and increasing amounts of RKIP. The '+feedback' condition in addition contained ERK which permits RKIP inactivation by ERK. The experiment is representative of three repeats and a quantification is shown on the right. The blue line represents MEK phosphorylation in the absence of ERK, i.e. the absence of feedback inhibition of RKIP. The red line indicates MEK phosphorylation in the presence of ERK where feedback is enabled. (D) Phosphorylated RKIP does not bind to Raf-1. Recombinant RKIP was phosphorylated by ERK in the presence of [γ-^{32}P]ATP as in B. Increasing amounts of RKIP (1.1 μg, 3.3 μg, 10 μg) were incubated with equal amounts of GST or GST–Raf-1 immobilized on glutathione-Sepharose beads. After washing the binding assay was separated by SDS-PAGE and bound RKIP was detected by immunoblotting, and phosphorylated RKIP was detected by autoradiography of the immunoblots. 'Input' contains 10% of the RKIP used in the binding assay.

persistently stimulated through PKC activation by TPA (Rubio et al., 2006), the deletion of the negative-feedback loop resulted in a non-oscillatory behavior of ppERK by inhibiting ERK-mediated SOS phosphorylation. ppERK levels increased monotonically with a significant change in the steady-state levels (Fig. 4A). For a transient stimulation of the pathway, the amplitude of ERK activation was decreased by the deletion of the positive-feedback loop, whereas the deletion of the negative-feedback loop slightly increased the amplitude and duration of ERK activation. Removal of RKIP had similar effects (Fig. 4B).

To further investigate the inhibitory effect of the positive-feedback loop, we completely removed RKIP. This not only eliminates the positive feedback but also the inhibitory actions of RKIP. With persistent stimulation, ppERK levels were higher and the rise time was also shorter compared with when the physical interaction of ERK and RKIP was inhibited and the oscillations were dampened (Fig. 4A). For a transient stimulation of Ras, the amplitude of the ERK-activation curve was increased and the rise time was shorter, similar to the effects observed with persistent stimulation (Fig. 4B).

In summary, these results suggest that the negative-feedback loop plays a crucial role in generating the oscillatory behavior and decreasing the amplitude of oscillations of ppERK levels. However, the positive-feedback loop seems to be involved in enhancing the oscillatory behavior and increasing the amplitude of ppERK oscillations. It has also a similar role for transient stimulation. In addition, the complete removal of RKIP accelerates the rise time, amplitude and duration of ERK activity, resulting in a more sustained activation under conditions of transient stimulation.

RKIP induces a switch-like behavior of MEK through the positive-feedback loop

The simulation results (Fig. 4) showed that RKIP has a profound impact on ERK activation. Experimental results also support the fact that the ERK pathway activity and its subsequent cellular functions are remarkably altered by the expression level of RKIP

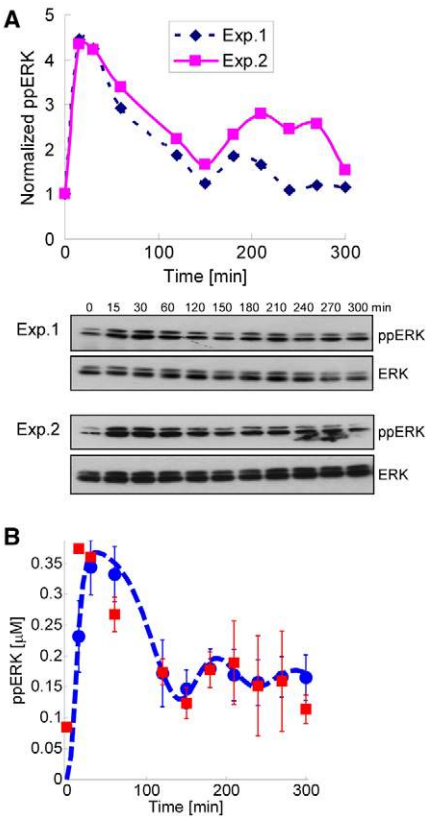

Fig. 3. Oscillations of ERK activity. (A) ERK activation profile in COS-1 cells in response to TPA treatment. Serum starved COS-1 cells were treated with 100 ng/ml TPA for the indicated time points. Cell lysates were immunoblotted with ppERK followed by ERK antibodies. Lower panel, western blots of two independent representative experiments. Upper panel, the blots were quantified by laser densitometry, ppERK was corrected for ERK loading, and plotted. (B) Comparison of biochemically measured with predicted ERK activation. The biochemically measured ERK activities from panel A are shown as red rectangles with the error bars corresponding to the s.d. from two independent experiments. The measured ERK activity was scaled down for comparison with the simulation data. The ERK activation profile predicted by the PSRA parameter estimation method is shown as dashed blue line obtained from a nominal parameter values (see Table 2). Blue circles with error bars denote in silico simulation data obtained from repeated simulations (n=50) over a 30% random variation of parameters.

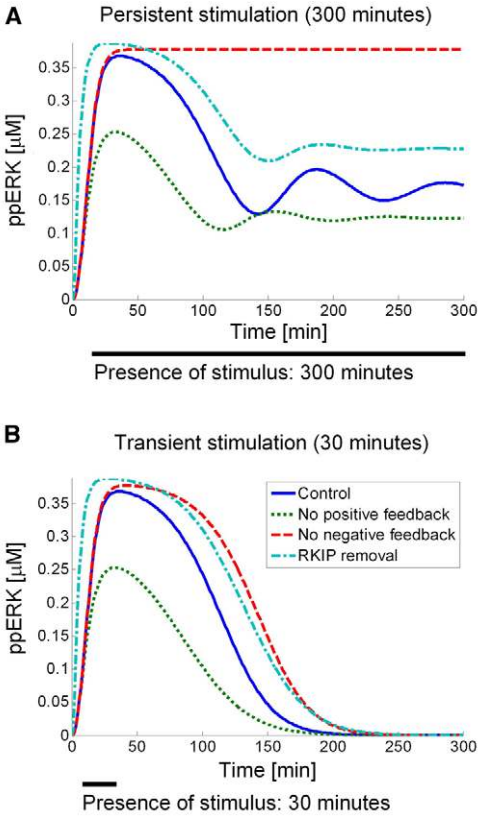

Fig. 4. Dynamic analysis of the positive- and negative-feedback mechanisms by computational simulation. 'No positive feedback' indicates that the positive-feedback loop has been removed by inhibiting ERK mediated RKIP phosphorylation. 'No negative feedback' indicates that the negative feedback loop has been removed by inhibiting ERK mediating SOS phosphorylation. 'RKIP removal' indicates that RKIP has been removed completely, eliminating both the positive feedback and the inhibitory action of RKIP. The control had none of the feedback loops or RKIP removed. (A) Simulations for persistent stimulations (300 minutes). (B) Simulations for transient stimulations (30 minutes).

protein (Chatterjee et al., 2004; Keller et al., 2004). To further examine the functional role of RKIP, we conducted simulations by increasing RKIP concentrations from 0 to 1.2 μM for a constant stimulation input. The oscillatory behaviors and amplitudes of oscillation of phosphorylated MEK (ppMEK) and ppERK levels were suppressed, along with the gradual increase of RKIP concentration (Fig. 5A,B). However, the amplitude of Raf activation curves was enhanced, whereas its oscillatory pattern disappeared as RKIP concentration increased (Fig. 5C). This is presumably due to the decreased negative-feedback effect, which allows Raf-1 activation to accumulate.

To further investigate the functional role of RKIP when the negative-feedback loop is deleted, we modified the mathematical model so that Raf-1 activity could be controlled independently of Ras, which eliminates the negative-feedback loop. This is achieved by simulating the expression of a constitutively active Raf-1 mutant, RafΔN, which lacks the N-terminal regulatory domain (including the Ras-binding domain), rendering the kinase domain catalytically active independent of Ras (Heidecker et al., 1990). However, RafΔN is still susceptible to inhibition by RKIP (Yeung et al., 1999). For a constant level of Raf-1 activity, the ppMEK levels were sigmoidally decreased as RKIP increased (Fig. 6A), whereas the oscillations of ppMEK levels disappeared, because the negative-feedback loop was deleted. Importantly, the steady-state response curves of MEK activation showed switch-like behavior (Fig. 6B).

To experimentally verify the switch-like behavior of ppMEK in response to an increase in RKIP levels, we transfected COS-1 cells with the constitutively active Raf-1 mutant, RafΔN, also termed BXB (Heidecker et al., 1990). Expression of RafΔN resulted in a steady state of sustained MEK activation. In addition, we transfected cells with an RKIP expression plasmid in increasing amounts that were carefully chosen to give a linear increase of RKIP protein levels in the transfected cells. RafΔN efficiently induced MEK activity as measured by MEK phosphorylation. MEK activation was not inhibited by increasing RKIP levels up to a certain threshold,

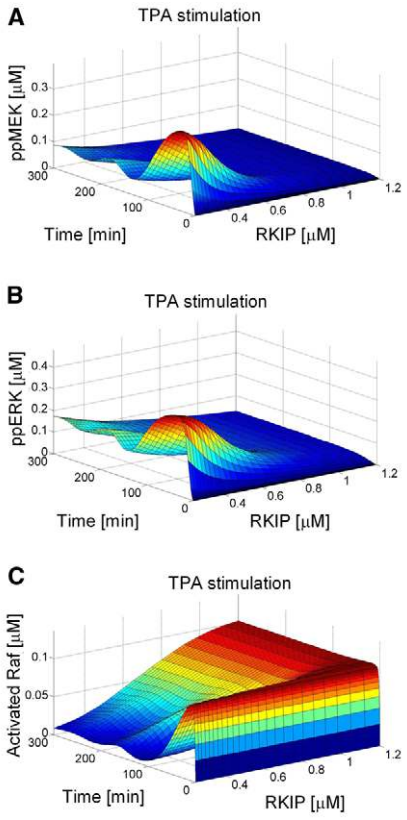

Fig. 5. RKIP regulates the oscillatory behavior of cellular responses. The oscillatory behaviors of ppMEK (A) and ppERK (B) are suppressed along with the increase of RKIP concentration. The oscillation amplitude of activated Raf-1 levels (C) is increased whereas the oscillatory pattern vanishes as RKIP concentration increases.

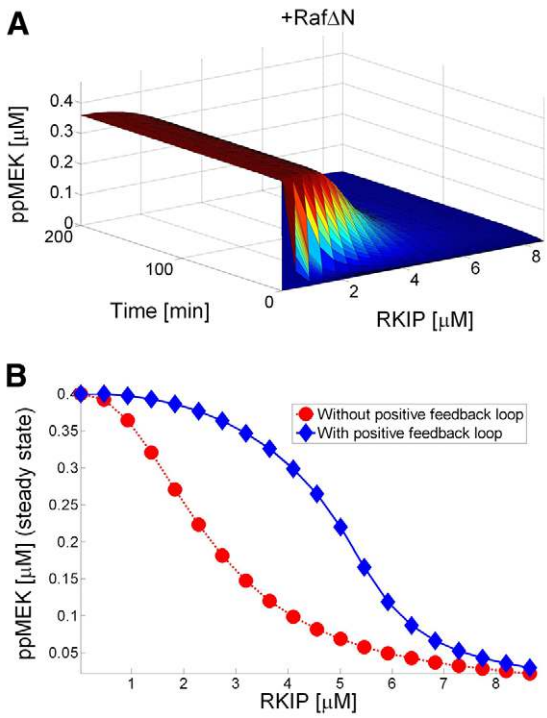

Fig. 6. RKIP induces a switch-like behavior of MEK activity. The mathematical model was modified such that Raf-1 activation could be controlled independent of upstream inputs. (A) Under conditions of constant Raf-1 activity achieved by simulating the expression of the constitutively active RafΔN the levels of ppMEK decreased sigmoidally as RKIP increased. (B) The steady-state response curves of ppMEK. The switch-like behavior in response to a gradual increase of RKIP levels disappeared when the positive-feedback loop was eliminated.

where a precipitous inhibition occurred (Fig. 7A). This switch-like behavior is unexpected for a stoichiometric inhibitor such as RKIP, but fully consistent with the in silico simulation results (Fig. 6B). It can be explained by the positive feedback that functionally compensates for increases in RKIP levels up to the point where high levels of RKIP sequester Raf effectively enough to cause MEK activation and the positive feedback to collapse.

To prove this point, we established stable cell lines with doxycycline-inducible expression of RKIP or RKIP S99A mutant protein (Fig. 7B). Inducing RKIP expression inhibited TPA activation of MEK with switch-like kinetics, whereas RKIP S99A (breaking the positive feedback resulting from mutation of the ERK phosphorylation site) caused the inhibition to become linear. In simulations, we found that the switch-like behavior of ppMEK is diminished by deletion of the positive-feedback loop (Fig. 6B). Taken together, these results suggest that the RKIP positive-feedback loop plays a crucial role in programming the switch-like behavior of MEK.

RKIP determines the dynamic characteristics of ERK

To characterize the functional role of RKIP in the regulation of the ERK pathway for varying stimulation strengths, we gradually increased the strength of stimulation at different constant concentrations of RKIP. At a low concentration of RKIP (0.24 μM), ppERK showed a dampened oscillatory behavior across the whole stimulation range (Fig. 8A). At a high RKIP concentration (0.96 μM) total initial ppERK levels were significantly suppressed compared with those observed under conditions of low RKIP expression. However, ppERK levels still increased in response to the increase of stimulation whereas the oscillations become strongly dampened (Fig. 8B). These results suggest that RKIP determines the dynamic characteristics of ERK depending on the stimulation strengths. In summary, when RKIP is low, ppERK increases enough to activate the negative-feedback loop, which leads to the oscillatory behavior; when RKIP becomes higher, ppERK is decreased and thus the negative-feedback loop is no longer effective, which leads to the weaker oscillatory behavior.

Discussion

Feedback loops in signaling pathways are known to have important roles in determining system dynamics. In particular, it is known that positive-feedback loops can induce switch-like or bistable behavior (Ferrell, 2002), whereas negative-feedback loops can contribute to system stability (Kholodenko, 2000). However, in principle, feedback loops can generate a wide diversity of behaviors, especially when they are interconnected (Cho et al., 2003a; Soyer et al., 2006). Thus, it was of importance to analyze the role and impact of the positive- and negative-feedback loops emanating from ERK for the dynamic behavior of the ERK pathway.

Direct experimental evidence for a positive-feedback loop initiated by ERK via inactivation of the inhibitor RKIP has not previously been reported. Here, we present evidence that ERK

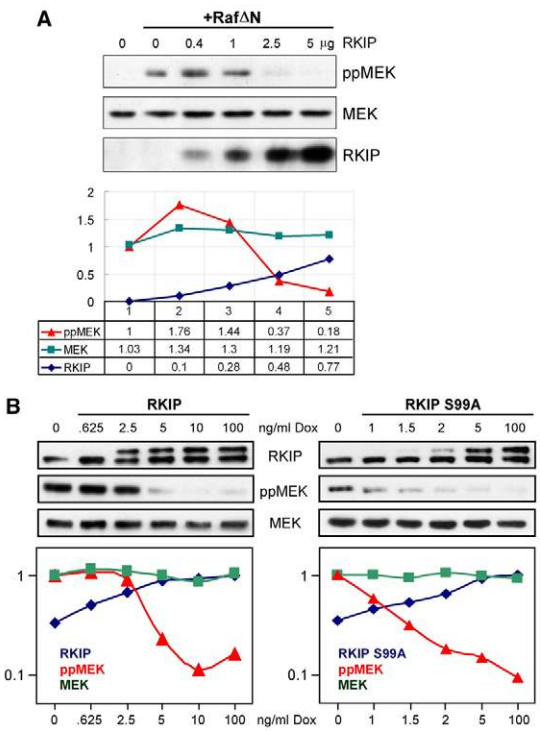

Fig. 7. Experimental verification of the switch-like behavior of phosphorylated MEK. (A) COS-1 cells were transfected with a constant amount of RafΔN in order to activate MEK and different amounts of RKIP plasmid as indicated in order to generate a linear increase in RKIP protein levels. Cells were lysed 2 days after transfection, and steady-state MEK activation was assayed by western blotting with phosphospecific MEK antibodies. Total levels of MEK and RKIP proteins were also assayed by western blotting. Quantification of blots by laser densitometry is shown below as normalized scan units. (B) LS174T colon cancer cell lines with a doxycycline (Dox)-regulatable Flag-RKIP or Flag-RKIP S99A expression system were induced with the indicated amounts of Dox to achieve a graded overexpression of RKIP. As a result of the Flag-tag, the induced RKIP migrates just above the endogenous RKIP band. Cells were stimulated with 10 ng/ml TPA for 15 minutes, ppMEK, MEK and RKIP levels were assayed by immunoblotting (upper panels) and quantified by laser densitometry (lower panels; expression is given as normalized scan units on a logarithmic scale). The experiment was repeated twice with consistent results.

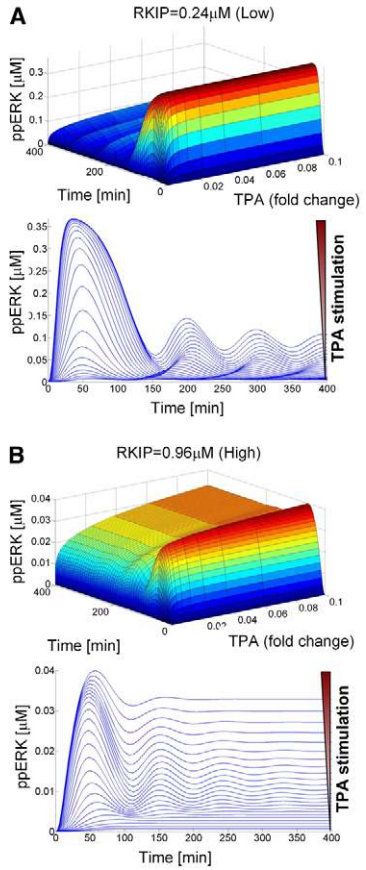

Fig. 8. RKIP determines the dynamics of phosphorylated ERK depending on stimulation strength. (A) At low RKIP concentrations ERK activity exhibits damped oscillations. (B) At a high RKIP concentration, total initial ppERK levels are significantly suppressed and the oscillations become dampened compared with those observed under conditions of low RKIP expression.

phosphorylates RKIP on S99 and give also an in-depth analysis of the functional consequences. The phosphorylation of RKIP by ERK generates a positive-feedback loop. Based on these observations, we have developed an experimentally validated mathematical model of the ERK pathway, including the positive- and negative-feedback loops, which allowed us to investigate the hidden dynamics of these feedback loops, and the functional role of RKIP. By contrast, the existence of a negative-feedback loop from ERK to SOS and Ras activation is well documented (Dong et al., 1996; Waters et al., 1995a), but the computational analysis of this feedback is not well developed (Orton et al., 2005). The existing analysis indicated an important role for this negative feedback in determining the duration of ERK activation (Brightman and Fell, 2000), but this prediction was purely theoretical and not validated by biochemical experimentation.

Our results indicate that under conditions of transient stimulation, the negative feedback mainly affects the duration of the signal, consistent with published results (Brightman and Fell, 2000). However, under conditions of chronic stimulation, the negative feedback assumes a major role in stabilizing the system response and in encoding oscillatory behavior. Our results show that ERK activity oscillations are slow and dampened. Thus, they occur outside the time-frame measured in most studies, and would thus have been overlooked. Oscillations in the ERK pathway caused by a negative-feedback loop from ERK to an upstream component of the pathway have been predicted on the grounds of theoretical analysis (Kholodenko, 2000). We now show that although the negative feedback from ERK to SOS is critical for oscillatory behavior, the positive feedback has an important role in modulating the amplitude and frequency of the oscillations. Thus, the ERK activity profile seems to be shaped by the composite effects of the negative feedback, the coupling with a positive feedback, the inhibitory function of RKIP and the strength of stimulation (see Fig. 8). The positive-feedback loop operating by ERK inactivating RKIP confers a switch-like behavior of MEK activity in response to the gradual increase of RKIP. Thus, RKIP seems to function as a rheostat that controls the amplitude of ERK signaling within a certain range. However, RKIP can also impinge on the oscillatory behavior caused by the negative feedback. An increase in RKIP concentration enhances the dampening of ppERK levels. These properties seem to make an ideal noise filter, because they would

permit the cell to interpret a signal both in terms of the oscillation frequency, as well as in terms of the switch to a sustained activation. In an organism, cells are constantly exposed to a deluge of growth factors and hormones, and the ability to distinguish true signals from noise is probably much more important than we currently appreciate. Thus, it is an appealing possibility that as a result of the combination of positive and negative feedbacks cells might sense transient stimulation in a fundamentally different manner to that observed under chronic stimulation. When the signal rises and wanes rapidly in response to a transient stimulation, it will probably depend on the rise time and amplitude of the signal, as to whether it can cross the noise threshold and evoke a biological decision. This seems appropriate for acute responses, which are designed to react to strong cues. Sustained stimulation that gives rise to oscillations might designate a decision-making phase, where the cell can integrate various other stimuli before committing to a biological decision. In this regard, the dampening of oscillations in response to singular stimuli could effectively filter out everything other than synergistic signals. If the stimulus is, however, chronic and strong, the oscillations eventually can transpose into a bistable switch, which can determine the fate of the cell. This hypothesis has wide ramifications for biochemistry and cell biology. Although our data are consistent with this hypothesis, further explorations in different systems will be needed.

It will be of particular interest to compare our data with observations from the PC12 cell system. PC12 is a rat cell line that proliferates in response to EGF and differentiates into neuron-like cells in response to nerve growth factor (NGF). Cell proliferation and differentiation are regulated by integrative operation of multiple pathways, and it is known that the ERK pathway has an important role in such regulation, with transient activity specifying proliferation and sustained activity triggering differentiation (Marshall, 1995). These distinct ERK dynamics are proposed to be caused by different feedback architectures or receptor-specific internal mechanisms. Sasagawa et al. suggested that the crucial difference of the ERK dynamics in PC12 cells depends on Ras and Rap1 activation, which are differently regulated by NGF and EGF stimulation (Sasagawa et al., 2005). Santos and co-workers suggested that the feedback topology of the ERK pathway dynamically adapts to different stimulations (Santos et al., 2007). EGF stimulation favors the configuration where negative feedback dominates and thus leads to transient ERK activation. By contrast, NGF promotes a positive-feedback topology leading to sustained ERK activation (Santos et al., 2007). Interestingly, these investigators suggested that the NGF-triggered positive feedback involves RKIP inactivation by PKC (Santos et al., 2007). It will be interesting to test our findings in this cell system, especially as our results extend these interpretations by indicating that it is the integration of positive- and negative-feedback mechanisms that shape ERK activation dynamics. Another interesting suggestion is that switch-like versus analogue modes of ERK activation could be encoded by the subcellular compartment where Raf-1 is activated. Raf-1 activation at the plasma membrane has been reported to produce a digital, switch-like acute activation of ERK, whereas activation of Raf-1 at the Golgi membrane results in an analogue and delayed activation of ERK (Inder et al., 2008; Tian et al., 2007). The role of the positive- and negative-feedback loops in these scenarios has not yet been explored. RKIP is mainly cytosolic, but is also recruited to the plasma membrane in the presence of activated Ras (Yeung et al., 1999), where it could contribute to the switch-like signaling by Raf-1. Ras activation at the Golgi seems to use different guanosine nucleotide exchange factors (Bivona et al., 2003), which would render the ppERK-mediated feedback to SOS irrelevant. In addition, the mechanism of Raf-1 activation at the plasma membrane might be different from that at the Golgi (Inder et al., 2008), and it is also unknown whether and how RKIP could affect the Raf-1 signaling emanating from the Golgi. Thus, an important and fertile avenue of future work will be to explore the connections between feedback loops and subcellular compartmentalization.

Most mathematical models of the ERK pathway have been constructed using nonlinear ordinary differential equations (ODEs). Once the structure of the mathematical model is determined, the next challenge will be to identify its kinetic parameters from experimental data. Parameter estimation for nonlinear systems remains a difficult task, although a number of techniques are available (Cho et al., 2003a; Cho et al., 2003b; Kutalik et al., 2004; Muller et al., 2002; Swameye et al., 2003). In most studies, parameter values for modeling are taken from the literature. As these data are often from different laboratories using different assay conditions and different cell lines, relatively large errors can occur in simulations because of incomparable experimental conditions. In such cases, it is impossible to discern whether the discrepancies between simulations and experimental observations are due to incorrect parameter values, non-homogeneous data sets or an inappropriate model structure. To avoid this 'modeling dilemma', we have developed a new method, termed the pseudo-random search algorithm (PRSA), based on previous random search techniques, which is described fully in the Materials and Methods section. Using the PRSA, we have estimated the parameter values from homogeneous time-series data of MEK and ERK in COS-1 cells. In addition, we have repeated the simulations over 30% random parameter variations to test parameter sensitivity. The simulation results were in agreement with the experimental results, thereby validating PRSA as a viable approach for parameter estimation. In summary, we suggest that the combination of positive- and negative-feedback loops are crucial to produce the dynamic characteristics of ERK activation.

Materials and Methods

Biochemical measurements in cells

COS-1 cells were grown in Dulbecco's Modified Minimal Medium plus high glucose supplemented with 10% fetal calf serum. Cells were transfected using Lipofectamine (Invitrogen) according to the manufacturer's instructions. To provide time-course data used for parameter estimation, 1×10^7 COS-1 cells were serum starved overnight and then stimulated with 100 ng/ml TPA for the indicated times. Cells were lysed in 2 ml RBD pull-down buffer (20 mM Tris-HCl pH 7.5, 150 mM NaCl, 1% Triton X-100, 0.5% deoxycholate, 0.1% SDS) supplemented with protease inhibitors (1 mM PMSF, 1 μg/ml Leupeptin). Crude lysates were cleared by pelleting the debris by centrifugation at 15,000 ***g*** for 5 minutes at 4°C. 10 μl of the cleared lysates were separated by SDS polyacrylamide gel electrophoresis (SDS-PAGE). The gel was blotted, and the blot was stained for ppMEK and ppERK, respectively, using specific antibodies (Cell Signaling) and enhanced chemiluminescent detection (ECL), according to the manufacturer's instructions (Roche). ECL signals were detected by autoradiography and scanned. Only non-saturated exposures were scanned and used for quantification. Then, the antibodies were removed by incubating the blot in stripping buffer (100 mM glycine pH 3, 3% SDS, 20 mM dithiothreitol) for 15 minutes at 25°C. Afterwards, the blots were re-stained with antibodies against MEK and ERK, respectively, as above, to assess the total amount of MEK and ERK. The scans were evaluated by laser densitometry using the NIH ImageJ (version 1.36b) software. These experiments were repeated three times.

Biochemical measurements in vitro

For in vitro experiments, recombinant proteins were used. Functional, kinase-competent Raf-1 was produced in Sf-9 insect cells and purified exactly as described previously (Hafner et al., 1994). Briefly, Sf-9 cells were infected with a GST-Raf-1 baculovirus at a multiplicity of infection (MOI) of 10, and cells were harvested 48 hours later by resuspension in lysis buffer (20 mM Tris-HCl, pH 7.4, 150 mM NaCl, 1% Triton X-100) supplemented with phosphatase and protease inhibitor cocktails

(Roche Diagnostics). If required, GST-Raf-1 was activated by co-infection with baculoviruses expressing mutant H-RasV12 and the tyrosine kinase Lck (both at MOI of 5). GST-Raf-1 was purified by adsorption to glutathione-Sepharose and three washes in lysis buffer. Then, the beads were equilibrated with thrombin digestion buffer (20 mM Tris-HCl pH 8.4, 150 mM NaCl, 2.5 mM $CaCl_2$) and Raf-1 was released by cleaving off the GST portion by thrombin. In the kinase assays, Raf-1 without the GST portion was used. Recombinant His-tagged MEK and ERK proteins were produced in *E. coli* and purified by Ni^{2+} chromatography, as described (Gardner et al., 1994). GST-RKIP was produced in *E. coli* and purified by adsorption to glutathione-Sepharose beads and subsequent removal of the GST portion by thrombin cleavage as described (Yeung et al., 2000). For in vitro activation and kinase assays, recombinant proteins were incubated in the indicated combinations in kinase buffer (20 mM Tris-HCl, pH 7.4, 20 mM NaCl, 10 mM $MgCl_2$, 1 mM DTT) supplemented with 20 μM ATP and 2 μCi [γ-^{32}P]ATP for 20 minutes. For the pre-activation experiments shown in Fig. 2A, Raf-1 was incubated with MEK (200 ng/ml), or MEK (200 ng/ml) and ERK (1 μg/ml) in the presence of 20 μM ATP for 20 minutes before 2 μCi [γ-^{32}P]ATP and recombinant RKIP (500 μg/ml) was added. For the in vitro RKIP phosphorylation experiment shown in Fig. 2B, ERK was activated by preincubation with activated Raf-1 and MEK in the presence of 20 μM ATP for 20 minutes before 2 μCi [γ-^{32}P]ATP and recombinant RKIP proteins (500 μg/ml) were added. For the in vitro MEK phosphorylation experiment shown in Fig. 2C, Raf-1 was incubated with recombinant MEK (200 ng/ml), or MEK (200 ng/ml) and ERK (1 μg/ml) in the presence of 20 μM ATP and increasing amounts of recombinant RKIP protein for 20 minutes. Phosphorylated MEK was detected by immunoblotting with a ppMEK-specific antibody (Cell Signaling) For the binding assays shown in Fig. 2D, GST-Raf-1 and GST as control, were expressed in Sf-9 cells and purified by adsorption to glutathione-Sepharose beads. Beads were washed in lysis buffer and equilibrated in kinase buffer before incubation with recombinant RKIP (500 μg/ml) that had been phosphorylated by activated ERK (prepared as described above) using 20 μM ATP and 2 μCi [γ-^{32}P]ATP. The total volume of the reaction was 20 μl.

Establishment and analysis of stable cell lines with inducible RKIP expression

Full-length *RKIP* with a 5′-single Flag tag was subcloned into pcDNA5/FRT. The S99A mutant was generated using the Quikchange Kit (Stratagene) with the primers RKIP S99A forward, 5′-AGGGCAATGACATCAGCGCTGGCACAGTCC-TCTCCG-3′ and RKIP S99A reverse, 5′-CGGAGAGGACTGTGCCAGCGCT-GATGTCATTGCCCT-3′. Full-length wild-type RKIP as well as the S99A mutant were transfected into the colon cancer cell line LS174T (van de Wetering et al., 2003) using an Amaxa Nucleofector (Amaxa, Cologne, Germany). For this, solution T and the program T-020 were used according to the manufacturer's protocol. Cells were selected with hygromycin B for 1 week. Then, clones were picked, expanded and expression of the RKIP constructs was checked with an anti-RKIP antibody (Upstate) after addition of doxycycline for 48 hours. Over-expression of both the wild-type RKIP as well as the S99A mutant was approximately twice that of the endogenous RKIP level. LS174T cells as well as the LS174-T-wtRKIP and LS174T-S99A RKIP were maintained in RPMI-1640 (Invitrogen) with 5% tetracycline-free FBS (PAA, Pasching, Austria) and 2 mM glutamine.

For the experiments shown in Fig. 7B, 50,000 cells were seeded in a six-well plate (Nunc). For regulated expression of RKIP, 0.5-100 ng/ml doxycycline (Sigma) was added to the medium as indicated. It should be noted that because of the inherently non-linear response kinetics of this inducible system, doxycycline concentrations need to be carefully titrated for each line in order to obtain graded expression profiles. 48 hours later, the normal growth medium was replaced and cells were starved overnight in medium containing 0.1% serum. Then 10 ng/ml TPA (Sigma) was added for 15 minutes before the cells were lysed in ice-cold lysis buffer (10 mM HEPES, pH 7.8, 1.5 mM $MgCl_2$, 10 mM KCl, 0.1% NP-40) supplemented with standard protease inhibitors (Sigma), incubated on ice for 10 minutes, and sonicated three times for 5 seconds. After centrifugation for 15 minutes at 10,000 ***g***, the supernatant was taken and protein concentrations were determined using the BCA protein assay kit (Pierce). Equal aliquots (20 μg) of protein per sample were separated by SDS-PAGE and immunoblotted as described above.

Construction of a mathematical model

Over past decades, an ever-increasing number of models of the ERK pathway have been developed, growing in both size and complexity (Orton et al., 2005; Schoeberl et al., 2002). These mathematical models have been used to investigate various biological behaviors such as dynamics of single feedback loops, oscillation, and signal specificity (Kholodenko, 2000). We developed a mathematical model of the ERK pathway based on the previous models by introducing the positive- and negative-feedback mechanisms, as well as the regulation of RKIP. The model structure was verified from experimental data in the literature. In this model we assumed that each protein kinase (i.e. Ras, Raf, MEK, ERK) has only two possible states: active and inactive, and that the total amount is conserved. The negative-feedback mechanism by which the SOS-Grb2 complex is dissociated by the active ERK was assumed to be allosteric inhibition, and only ERK is considered as a SOS kinase. Both ERK (Langlois et al., 1995) and RSK2 (Douville and Downward, 1997) have been proposed as kinases that phosphorylate SOS and mediate the negative feedback. This simplification seems appropriate because RSK2 is directly activated by ERK (Yoon and Seger, 2006). The dissociation of the RKIP-Raf complex by phosphorylation was modeled as competitive inhibition because the kinetic analysis of MEK phosphorylation by Raf-1 revealed that RKIP diminished only the K_m value (i.e. Michaelis-Menten coefficient) but not the V_{max} (i.e. maximum velocity) of the reaction (Yeung et al., 2000).

$$\frac{d[RasGTP]}{dt} = \frac{K_{cat\_1}u(t)\left(\overline{Ras}-[RasGTP]\right)}{\left(K_{mk\_1}+\left(\overline{Ras}-[RasGTP]\right)\right)\left(1+\left(\frac{[ppERK]}{K_{i\_erk}}\right)^{3.2}\right)}-\frac{V_{max\_1}[RasGTP]}{K_{mp\_1}+[RasGTP]} \quad (1)$$

$$\frac{d[Raf^*]}{dt}=\frac{K_{cat\_2}\left(\overline{Raf}-[Raf^*]\right)[RasGTP]}{K_{mk\_2}+\left(\overline{Raf}-[Raf^*]\right)}-\frac{V_{max\_2}[Raf^*]}{K_{mp\_2}+[Raf^*]} \quad (2)$$

$$\frac{d[ppMEK]}{dt} = \frac{K_{cat\_3}\left(\overline{MEK}-[ppMEK]\right)[Raf^*]}{K_{mk\_3}\left(1+\left(\frac{\left(\overline{RKIP}-[pRKIP]\right)}{K_{i\_rkip}}\right)^{2.3}\right)+\left(\overline{MEK}-[ppMEK]\right)}-\frac{V_{max\_3}[ppMEK]}{K_{mp\_3}+[ppMEK]} \quad (3)$$

$$\frac{d[ppERK]}{dt}=\frac{K_{cat\_4}\left(\overline{ERK}-[ppERK]\right)[ppMEK]}{K_{mk\_4}+\left(\overline{ERK}-[ppERK]\right)}-\frac{V_{max\_4}[ppERK]}{K_{mp\_4}+[ppERK]} \quad (4)$$

$$\frac{d[pRKIP]}{dt}=\frac{K_{cat\_5}\left(\overline{RKIP}-[pRKIP]\right)[ppERK]}{K_{mk\_5}+\left(\overline{RKIP}-[pRKIP]\right)}-\frac{V_{max\_5}[pRKIP]}{K_{mp\_5}+[pRKIP]}, \quad (5)$$

where [*RasGTP*] and [*Raf**] denote the activated forms of Ras and Raf, respectively. [*ppMEK*] and [*ppERK*] denote the activated forms of MEK and ERK, respectively. [*pRKIP*] denotes the phosphorylated form of RKIP. The upper bar of each protein kinase (e.g. $\overline{ERK}$) denotes the total amount of the protein which is assumed constant. $u(t)$ denotes the activating stimulation.

Parameter estimation

Parameter estimation means to find the maximum likelihood parameters that minimize the discrepancy between experimental data and simulated data obtained from a mathematical model. The cost function (J) for parameter estimation is defined (Peifer and Timmer, 2007) by

$$J(\boldsymbol{p})=\sum_{j=1}^{M}\sum_{i=1}^{N}\left(\frac{\bar{y}_{j,i}-y_j(t_i,\boldsymbol{p})}{\sigma_{j,i}}\right)^2, \quad (6)$$

where M is the number of given experimental data and N is the number of time points of each experimental data. The output of the mathematical model $y_j(t_i,\boldsymbol{p})$ is the value of the solution y_j of the ordinary differential equation (ODE) system at t_i with parameter set $\boldsymbol{p}$ and $\bar{y}_{j,i}$ is the mean of given repeated measurements of signaling molecules corresponding to y_j at t_i with the error variance $\sigma_{j,i}$.

Parameter estimation of a system represented by nonlinear ODEs is still a difficult task because no analytical form of the solution is available in general. Therefore, the parameter estimation of a model from given experimental data is usually carried out iteratively, starting from some initial guess. Estimated parameters are updated at each iteration loop such that the difference between the simulated data and given experimental data is minimized. This update step is implemented based on the gradient of an object function. In this case, steepest descent methods might become

Table 1. Parameter sensitivity analysis*

Parameter (P_j)	Sensitivity function (S_j) with respect to different parameter perturbations (ΔP_j)			Average
	ΔP_j =10%	ΔP_j =20%	ΔP_j =30%	
K_{i_rkip}	0.501	0.510	0.518	0.510
K_{i_erk}	0.486	0.488	0.485	0.486
V_{max_4}	0.489	0.484	0.478	0.484
K_{mk_4}	0.465	0.473	0.485	0.474
K_{mp_4}	0.486	0.474	0.461	0.474
K_{cat_4}	0.466	0.472	0.480	0.473
V_{max_1}	0.495	0.463	0.420	0.459
K_{mp_1}	0.490	0.449	0.391	0.443
V_{max_2}	0.349	0.341	0.328	0.339
K_{mp_2}	0.346	0.332	0.314	0.331
V_{max_3}	0.329	0.323	0.314	0.322
K_{mp_3}	0.329	0.323	0.314	0.322
K_{cat_3}	0.282	0.285	0.290	0.285
K_{mk_3}	0.281	0.285	0.290	0.285
K_{mk_2}	0.215	0.216	0.221	0.217
K_{mk_5}	0.214	0.216	0.220	0.217
K_{cat_2}	0.215	0.216	0.217	0.216
K_{cat_5}	0.213	0.214	0.215	0.214
V_{max_5}	0.208	0.210	0.213	0.210
K_{mp_5}	0.208	0.208	0.208	0.208
K_{cat_1}	0.151	0.151	0.154	0.152
K_{mk_1}	0.112	0.114	0.114	0.113

*Each parameter was perturbed with 10-30% variations. We found that K_{i_rkip}, K_{i_erk}, V_{max_4}, K_{mk_4}, K_{mp_4}, K_{cat_4}, V_{max_1} and K_{mp_1} have pronounced effects on ppERK dynamics.

trapped into a local minimum and never reach a global minimum (Moles et al., 2003). However, a random search technique effectively probes the whole parameter space to minimize a given cost function (Khorasheh et al., 1999; Moles et al., 2003) and this includes genetic algorithms (Lee et al., 2006; Paterakis et al., 1998). In this study, we have developed a new parameter estimation method, a pseudo-random search algorithm (PRSA), as one of such random search techniques. PRSA is summarized by the following steps: (0) Guess the initial values (seeds) of parameters to be estimated. (1) Set the range of each parameter such that the upper and lower boundaries are set to be 1.5-fold and 0.5-fold of the seed, respectively. These upper and lower boundaries can be adjusted, if needed. (2) Make a pool of K+2 values for each parameter: K parameter values are chosen within the parameter range, one is randomly selected out of the range to prevent this algorithm from trapping into a local minimum, and the other is set to the seed value to prevent non-converging oscillations near the minimum. (3) Simulate the model for all possible combinations of parameter values in the pool and compute the corresponding cost function. (4) Determine a set of the parameter values at which the cost function is minimal. This minimum value is to be called a 'local cost value'. (5) Replace the seeds in Step 1 with the parameter values determined in Step 4. (6) Iterate Steps 1-5 until the local cost values converge to a steady-state point. The parameter values at which the local cost value is minimal are considered to be the maximum-likelihood parameters.

The computational complexity of PRSA is order of $R(K+2)^N$ where R is the number of iterations (through Steps 1-5), K+2 is the size of each parameter pool, and N is the number of parameters to be estimated. This implies that the complexity becomes exponentially increased along with the number of parameters. So, in the case of a large number of parameters, we further employ the following procedures.

Initial estimation

We cluster n parameters into m ($m \leqslant n$) sets according to their influence on a system output and consider cluster parameters representing their clusters. In this case, we have generated random pairs of parameters to compare their influences on ppERK dynamics and then clustered 16 parameters (out of 22 parameters in total) into the following four sets: $C_1=\{K_{cat\_1}, K_{cat\_2}, K_{cat\_3}, K_{cat\_5}\}$, $C_2=\{V_{max\_1}, V_{max\_2}, V_{max\_3}, V_{max\_4}\}$, $C_3=\{K_{mp\_1}, K_{mp\_2}, K_{mp\_3}, K_{mp\_4}, K_{mp\_5}\}$, $C_4=\{K_{mk\_1}, K_{mk\_4}, K_{mk\_5}\}$. Then, we considered four representative cluster parameters, $K_{cat} \in C_1$, $V_{max} \in C_2$, $K_{mp} \in C_3$ and $K_{mk} \in C_4$ for each set, respectively. Together with non-clustered parameters (K_{cat_4}, V_{max_5}, K_{mk_1}, V_{max_3}, K_{i_rkip}, K_{i_erk}), we now have ten parameters to be estimated and applied the PRSA. The parameter estimates obtained in this step are used as nominal values in the following procedures.

Sensitivity analysis

We identify parameters having relatively significant effects on ppERK dynamics using sensitivity analysis. The sensitivity function $S_j = \int s_j(t)dt$ is defined as follows:

$$s_j(t) = \frac{\frac{\partial O(t)}{O(t)}}{\frac{\partial P_j}{P_j}} \approx \frac{\frac{O(P_j + \Delta P_j, t) - O(P_j - \Delta P_j, t)}{O(P_j, t)}}{\frac{2\Delta P_j}{P_j}}, \quad (8)$$

where $O(t)$ is the model output (ppERK level) at time t and ΔP_j is a small perturbation of the j-th parameter P_j. From sensitivity analysis, we found that K_{i_rkip}, K_{i_erk}, V_{max_4}, K_{mk_4}, K_{cat_4}, V_{max_1} and K_{mp_1} have relatively significant effects on the ppERK dynamics (see Table 1 for details).

Fine tuning

Finally, we estimate the parameters chosen from sensitivity analysis using PRSA to optimize the goodness-of-fit to the experimental data. The parameter estimates are summarized in Table 2. The simulation results based on these parameter estimates correlate well with the time course data of the biochemical experiments (Fig. 3B). Thus, the mathematical model is quantitatively validated with the experimental data. We further confirmed that these behaviors are robust over random parameter variations (30%) with respect to the obtained parameter estimates.

This work was supported by the Korea Science and Engineering Foundation (KOSEF) grant funded by the Korea Ministry of Education, Science & Technology through the Systems Biology grant (M10503010001-07N030100112), the Nuclear Research grant (M20708000001-07B0800-00110), and the 21C Frontier Microbial Genomics and Application Center Program (Grant MG08-0205-4-0). The W.K. lab is supported by Cancer Research UK and B.M. was funded by a grant from the Association of International Cancer Research (AICR).

Table 2. Parameters used for in silico simulations*

K_{cat_1} (μM^{-1}minute^{-1})	K_{mk_1} (μM)	V_{max_1} (μM minute^{-1})	K_{mp_1} (μM)	K_{i_erk} (μM)
144	1.0	7.56	125.64	0.004
K_{cat_2} (μM^{-1}minute^{-1})	K_{mk_2} (μM)	V_{max_2} (μM minute^{-1})	K_{mp_2} (μM)	
144	90	7.56	95	
K_{cat_3} (μM^{-1}minute^{-1})	K_{mk_3} (μM)	V_{max_3} (μM minute^{-1})	K_{mp_3} (μM)	K_{i_rkip} (μM)
144	11	7.56	95	0.07
K_{cat_4} (μM^{-1}minute^{-1})	K_{mk_4} (μM)	V_{max_4} (μM minute^{-1})	K_{mp_4} (μM)	
53.52	136.88	20.11	191.079	
K_{cat_5} (μM^{-1}minute^{-1})	K_{mk_5} (μM)	V_{max_5} (μM minute^{-1})	K_{mp_5} (μM)	
144	90	28.8	95	
Ras (μM)	*Raf* (μM)	*MEK* (μM)	*ERK* (μM)	*RKIP* (μM)
0.35	0.12	0.36	0.7	0.24

*These were estimated from the in vitro experimental data of COS-1 cells using PRSA. The total amount of Raf, MEK, ERK and RKIP were measured in COS-1 cells and the total Ras level was taken from previous experimental data (Schoeberl et al., 2002).

References

Al-Mulla, F., Hagan, S., Behbehani, A. I., Bitar, M. S., George, S. S., Going, J. J., Garcia, J. J., Scott, L., Fyfe, N., Murray, G. I. et al. (2006). Raf kinase inhibitor protein expression in a survival analysis of colorectal cancer patients. *J. Clin. Oncol.* **24**, 5672-5679.

Bivona, T. G., Perez De Castro, I., Ahearn, I. M., Grana, T. M., Chiu, V. K., Lockyer, P. J., Cullen, P. J., Pellicer, A., Cox, A. D. and Philips, M. R. (2003). Phospholipase Cgamma activates Ras on the Golgi apparatus by means of RasGRP1. *Nature* **424**, 694-698.

Brightman, F. A. and Fell, D. A. (2000). Differential feedback regulation of the MAPK cascade underlies the quantitative differences in EGF and NGF signalling in PC12 cells. *FEBS Lett.* **482**, 169-174.

Chatterjee, D., Bai, Y., Wang, Z., Beach, S., Mott, S., Roy, R., Braastad, C., Sun, Y., Mukhopadhyay, A., Aggarwal, B. B. et al. (2004). RKIP sensitizes prostate and breast cancer cells to drug-induced apoptosis. *J. Biol. Chem.* **279**, 17515-17523.

Cho, K. H., Shin, S. Y., Kim, H. W., Wolkenhauer, O., McFerran, B. and Kolch, W. (2003a). Mathematical modeling of the influence of RKIP on the ERK signaling pathway. *Comput. Methods Syst. Biol. CSMB*, 127-141.

Cho, K. H., Shin, S. Y., Lee, H. W. and Wolkenhauer, O. (2003b). Investigations into the analysis and modeling of the TNF alpha-mediated NF-kappa B-signaling pathway. *Genome Res.* **13**, 2413-2422.

Corbit, K. C., Trakul, N., Eves, E. M., Diaz, B., Marshall, M. and Rosner, M. R. (2003). Activation of Raf-1 signaling by protein kinase C through a mechanism involving Raf kinase inhibitory protein. *J. Biol. Chem.* **278**, 13061-13068.

Dong, C., Waters, S. B., Holt, K. H. and Pessin, J. E. (1996). SOS phosphorylation and disassociation of the Grb2-SOS complex by the ERK and JNK signaling pathways. *J. Biol. Chem.* **271**, 6328-6332.

Douville, E. and Downward, J. (1997). EGF induced SOS phosphorylation in PC12 cells involves P90 RSK-2. *Oncogene* **15**, 373-383.

Eblen, S. T., Slack-Davis, J. K., Tarcsafalvi, A., Parsons, J. T., Weber, M. J. and Catling, A. D. (2004). Mitogen-activated protein kinase feedback phosphorylation regulates MEK1 complex formation and activation during cellular adhesion. *Mol. Cell. Biol.* **24**, 2308-2317.

Ferrell, J. E., Jr (2002). Self-perpetuating states in signal transduction: positive feedback, double-negative feedback and bistability. *Curr. Opin. Cell Biol.* **14**, 140-148.

Fu, Z., Smith, P. C., Zhang, L., Rubin, M. A., Dunn, R. L., Yao, Z. and Keller, E. T. (2003). Effects of raf kinase inhibitor protein expression on suppression of prostate cancer metastasis. *J. Natl. Cancer Inst.* **95**, 878-889.

Gardner, A. M., Lange-Carter, C. A., Vaillancourt, R. R. and Johnson, G. L. (1994). Measuring activation of kinases in mitogen-activated protein kinase regulatory network. *Methods Enzymol.* **238**, 258-270.

Hafner, S., Adler, H. S., Mischak, H., Janosch, P., Heidecker, G., Wolfman, A., Pippig, S., Lohse, M., Ueffing, M. and Kolch, W. (1994). Mechanism of inhibition of Raf-1 by protein kinase A. *Mol. Cell. Biol.* **14**, 6696-6703.

Hagan, S., Al-Mulla, F., Mallon, E., Oien, K., Ferrier, R., Gusterson, B., Garcia, J. J. and Kolch, W. (2005a). Reduction of Raf-1 kinase inhibitor protein expression correlates with breast cancer metastasis. *Clin. Cancer Res.* **11**, 7392-7397.

Hagan, S., Garcia, R., Dhillon, A. and Kolch, W. (2005b). Raf kinase inhibitor protein regulation of raf and MAPK signaling. *Methods Enzymol.* **407**, 248-259.

Heidecker, G., Huleihel, M., Cleveland, J. L., Kolch, W., Beck, T. W., Lloyd, P., Pawson, T. and Rapp, U. R. (1990). Mutational activation of c-raf-1 and definition of the minimal transforming sequence. *Mol. Cell. Biol.* **10**, 2503-2512.

Inder, K., Harding, A., Plowman, S. J., Philips, M. R., Parton, R. G. and Hancock, J. F. (2008). Activation of the MAPK module from different spatial locations generates distinct system outputs. *Mol. Biol. Cell* **19**, 4776-4784.

Keller, E. T., Fu, Z. and Brennan, M. (2004). The role of Raf kinase inhibitor protein (RKIP) in health and disease. *Biochem. Pharmacol.* **68**, 1049-1053.

Kholodenko, B. N. (2000). Negative feedback and ultrasensitivity can bring about oscillations in the mitogen-activated protein kinase cascades. *Eur. J. Biochem.* **267**, 1583-1588.

Khorasheh, F., Ahmadi, A. M. and Gerayeli, A. (1999). Application of direct search optimization for pharmacokinetic parameter estimation. *J. Pharm Pharm. Sci.* **2**, 92-98.

Kolch, W. (2000). Meaningful relationships: the regulation of the Ras/Raf/MEK/ERK pathway by protein interactions. *Biochem. J.* **351**, 289-305.

Kolch, W. (2002). Ras/Raf signalling and emerging pharmacotherapeutic targets. *Expert Opin. Pharmacother.* **3**, 709-718.

Kolch, W. (2005). Coordinating ERK/MAPK signalling through scaffolds and inhibitors. *Nat. Rev. Mol. Cell. Biol.* **6**, 827-837.

Kolch, W., Calder, M. and Gilbert, D. (2005). When kinases meet mathematics: the systems biology of MAPK signalling. *FEBS Lett.* **579**, 1891-1895.

Kutalik, Z., Cho, K. H. and Wolkenhauer, O. (2004). Optimal sampling time selection for parameter estimation in dynamic pathway modeling. *Biosystems* **75**, 43-55.

Langlois, W. J., Sasaoka, T., Saltiel, A. R. and Olefsky, J. M. (1995). Negative feedback regulation and desensitization of insulin- and epidermal growth factor-stimulated p21ras activation. *J. Biol. Chem.* **270**, 25320-25323.

Lee, Y. H., Park, S. K. and Chang, D. E. (2006). Parameter estimation using the genetic algorithm and its impact on quantitative precipitation forecast. *Ann. Geophys.* **24**, 3185-3189.

Markevich, N. I., Hoek, J. B. and Kholodenko, B. N. (2004). Signaling switches and bistability arising from multisite phosphorylation in protein kinase cascades. *J. Cell Biol.* **164**, 353-359.

Marshall, C. J. (1995). Specificity of receptor tyrosine kinase signaling: transient versus sustained extracellular signal-regulated kinase activation. *Cell* **80**, 179-185.

Moles, C. G., Mendes, P. and Banga, J. R. (2003). Parameter estimation in biochemical pathways: a comparison of global optimization methods. *Genome Res.* **13**, 2467-2474.

Muller, T. G., Noykova, N., Gyllenberg, M. and Timmer, J. (2002). Parameter identification in dynamical models of anaerobic waste water treatment. *Math. Biosci.* **177-178**, 147-160.

Nakayama, K., Satoh, T., Igari, A., Kageyama, R. and Nishida, E. (2008). FGF induces oscillations of Hes1 expression and Ras/ERK activation. *Curr. Biol.* **18**, 332-334.

Orton, R. J., Sturm, O. E., Vyshemirsky, V., Calder, M., Gilbert, D. R. and Kolch, W. (2005). Computational modelling of the receptor-tyrosine-kinase-activated MAPK pathway. *Biochem. J.* **392**, 249-261.

Paterakis, E., Petridis, V. and Kehagias, A. (1998). Genetic algorithm in parameter estimation of nonlinear dynamic systems. *Lect. Notes Comput. Sci.* **1498**, 1008-1017.

Peifer, M. and Timmer, J. (2007). Parameter estimation in ordinary differential equations for biochemical processes using the method of multiple shooting. *IET Syst. Biol.* **1**, 78-88.

Rubio, I., Rennert, K., Wittig, U., Beer, K., Durst, M., Stang, S. L., Stone, J. and Wetzker, R. (2006). Ras activation in response to phorbol ester proceeds independently of the EGFR via an unconventional nucleotide-exchange factor system in COS-7 cells. *Biochem. J.* **398**, 243-256.

Santos, S. D., Verveer, P. J. and Bastiaens, P. I. (2007). Growth factor-induced MAPK network topology shapes Erk response determining PC-12 cell fate. *Nat. Cell Biol.* **9**, 324-330.

Sasagawa, S., Ozaki, Y., Fujita, K. and Kuroda, S. (2005). Prediction and validation of the distinct dynamics of transient and sustained ERK activation. *Nat. Cell Biol.* **7**, 365-373.

Schoeberl, B., Eichler-Jonsson, C., Gilles, E. D. and Muller, G. (2002). Computational modeling of the dynamics of the MAP kinase cascade activated by surface and internalized EGF receptors. *Nat. Biotechnol.* **20**, 370-375.

Schuierer, M. M., Bataille, F., Hagan, S., Kolch, W. and Bosserhoff, A. K. (2004). Reduction in Raf kinase inhibitor protein expression is associated with increased Ras-extracellular signal-regulated kinase signaling in melanoma cell lines. *Cancer Res.* **64**, 5186-5192.

Soyer, O. S., Salathe, M. and Bonhoeffer, S. (2006). Signal transduction networks: topology, response and biochemical processes. *J. Theor. Biol.* **238**, 416-425.

Swameye, I., Muller, T. G., Timmer, J., Sandra, O. and Klingmuller, U. (2003). Identification of nucleocytoplasmic cycling as a remote sensor in cellular signaling by databased modeling. *Proc. Natl. Acad. Sci. USA* **100**, 1028-1033.

Tian, T., Harding, A., Inder, K., Plowman, S., Parton, R. G. and Hancock, J. F. (2007). Plasma membrane nanoswitches generate high-fidelity Ras signal transduction. *Nat. Cell Biol.* **9**, 905-914.

van de Wetering, M., Oving, I., Muncan, V., Pon Fong, M. T., Brantjes, H., van Leenen, D., Holstege, F. C., Brummelkamp, T. R., Agami, R. and Clevers, H. (2003). Specific inhibition of gene expression using a stably integrated, inducible small-interfering-RNA vector. *EMBO Rep.* **4**, 609-615.

Waters, S. B., Holt, K. H., Ross, S. E., Syu, L. J., Guan, K. L., Saltiel, A. R., Koretzky, G. A. and Pessin, J. E. (1995a). Desensitization of Ras activation by a feedback disassociation of the SOS-Grb2 complex. *J. Biol. Chem.* **270**, 20883-20886.

Waters, S. B., Yamauchi, K. and Pessin, J. E. (1995b). Insulin-stimulated disassociation of the SOS-Grb2 complex. *Mol. Cell. Biol.* **15**, 2791-2799.

Wellbrock, C., Karasarides, M. and Marais, R. (2004). The RAF proteins take centre stage. *Nat. Rev. Mol. Cell. Biol.* **5**, 875-885.

Yeung, K., Seitz, T., Li, S., Janosch, P., McFerran, B., Kaiser, C., Fee, F., Katsanakis, K. D., Rose, D. W., Mischak, H. et al. (1999). Suppression of Raf-1 kinase activity and MAP kinase signalling by RKIP. *Nature* **401**, 173-177.

Yeung, K., Janosch, P., McFerran, B., Rose, D. W., Mischak, H., Sedivy, J. M. and Kolch, W. (2000). Mechanism of suppression of the Raf/MEK/extracellular signal-regulated kinase pathway by the raf kinase inhibitor protein. *Mol. Cell. Biol.* **20**, 3079-3085.

Yoon, S. and Seger, R. (2006). The extracellular signal-regulated kinase: multiple substrates regulate diverse cellular functions. *Growth Factors* **24**, 21-44.